Toxicology in Vitro 98 (2024) 105837

Contents lists available at ScienceDirect

Toxicology in Vitro

journal homepage: www.elsevier.com/locate/toxinvit

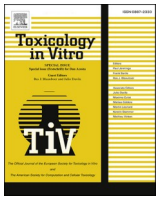

Silver nanoparticles induce formation of multi-protein aggregates that contain cadherin but do not colocalize with nanoparticles

Kaden M. Thomas, Nadja Spitzer *

Department of Biological Sciences, Marshall University, One John Marshall Dr., Huntington, WV, USA

ARTICLE INFO

Keywords:
Hyperspectral microscopy
Focal adhesions
Multi-protein aggregates
Sequestration
Nanotoxicology

ABSTRACT

Silver nanoparticles (AgNPs) are increasingly incorporated in diverse products to confer antimicrobial properties. They are released into the environment during manufacture, after disposal, and from the products during use. Because AgNPs bioaccumulate in brain, it is important to understand how they interact with neural cell physiology. We found that the focal adhesion (FA)-associated protein cadherin aggregated in a dose-dependent response to AgNP exposure in differentiating cultured B35 neuroblastoma cells. These aggregates tended to colocalize with F-actin inclusions that form in response to AgNP and also contain β-catenin. However, using hyperspectral microscopy, we demonstrate that these multi-protein aggregates did not colocalize with the AgNPs themselves. Furthermore, expression and organization of the FA protein vinculin did not change in cells exposed to AgNP. Our findings suggest that AgNPs activate an intermediate mechanism which leads to formation of aggregates *via* specific protein-protein interactions. Finally, we detail the changes in hyperspectral profiles of AgNPs during different stages of cell culture and immunocytochemistry processing. AgNPs in citrate-stabilized solution present mostly blue with some rainbow spectra and these are maintained upon mounting in Prolong Gold. Exposure to tissue culture medium results in a uniform green spectral shift that is not further altered by fixation and protein block steps of immunocytochemistry.

1. Introduction

Silver nanoparticles (AgNP) possess strong antimicrobial properties and are not cytotoxic to eukaryotic cells at low concentration (1–5 μg/ml) (Haase et al., 2012; Hadrup et al., 2012), making them useful as an antimicrobial in healthcare products, textiles, household appliances, and other consumer industries. As of 2011, AgNPs were the most identified nanotechnology material used in manufacturing (Samberg and Monteiro-Riviere, 2014). Global market value for AgNPs is anticipated to increase at a rate of 15% per year over the next decade (Spherical Insights Global Silver Nanoparticles Market, 2023). AgNPs can accumulate in the environment, potentially leading to low-level consumer and wildlife exposure. They disrupt gill breathing mechanisms and produce spinal cord deformities and cardiac arrhythmia in embryonic fish (Fabrega et al., 2011). In experimental mammals, AgNPs cross the blood-brain barrier and bioaccumulate in the brain causing neuronal damage (Recordati et al., 2021; Tang et al., 2010). Low-levels of AgNPs disrupt important dynamics of neuron proliferation (Liu et al., 2015) and differentiation in rats (Guo et al., 2017). Human exposure to AgNPs from packaging materials is estimated at 0.06–13 μg/day, and the concentration of AgNPs in aquatic ecosystems is estimated in the ng/l range (Sun et al., 2016; Gottschalk et al., 2013; McGillicuddy et al., 2017). Chronic exposure of organisms in and around outdoor microcosms dosed with a total of ~740 ng AgNP/ml led to bioaccumulation of Ag up to 1–1000 mg/kg (~μg/ml) after 30 days or a year (Colman et al., 2018). In carp, AgNPs accumulate to 25 μg/g (~μg/ml) in liver and 3 μg/g in muscle after exposure to 90 ng/ml AgNP for 20 days (Kakakhel et al., 2021). Therefore, given the bioaccumulation and long persistence of AgNPs in brain tissue (Recordati et al., 2021; Lee et al., 2013; Tang et al., 2008; van der Zande et al., 2012; Skalska et al., 2015; Skalska et al., 2020), experimental doses up to 5 μg/ml can reasonably be expected to represent bioaccumulated load. Concentrations of AgNPs below 5 μg/ml do not cause cell death in cultured cortical neurons (Xu et al., 2013) or PC12 cells (Hadrup et al., 2012). We previously found that although 1 μg/ml did not induce DNA fragmentation, this dose disrupted cytoskeletal organization, intracellular signaling pathways, and neurite extension in cultured adult neural progenitor and B35 cells (Cooper and Spitzer, 2015; Cooper et al., 2019; Spitzer et al., 2021). We therefore

* Corresponding author.
E-mail address: spitzern@marshall.edu (N. Spitzer).

https://doi.org/10.1016/j.tiv.2024.105837
Received 7 November 2023; Received in revised form 24 April 2024; Accepted 28 April 2024
Available online 30 April 2024

chose doses of AgNP at 0–4 μg/ml to investigate the physiological changes in neuronal cells in response to sub-lethal, environmentally relevant levels of exposure. Previously we showed that filamentous actin (F-actin) cytoskeletal structure is disrupted in cultured differentiating neural stem cells and B35 neuroblastoma cells. AgNP-exposed cells form F-actin inclusions reminiscent of those observed when cells are exposed to cytoskeletal toxins (Lazaro-Dieguez et al., 2008; Muller et al., 2013). These cells also exhibited neurite collapse and loss of neurite branching within an hour of exposure to AgNPs (Cooper and Spitzer, 2015). We further determined that F-actin inclusions co-localized with aggregates of β-catenin (Cooper et al., 2019), a signaling molecule that regulates neurite outgrowth and focal adhesions (FAs) (Tang et al., 2010; Lee et al., 2014; Yu and Malenka, 2003). β-catenin expression levels were reduced in cells treated with AgNPs and our pharmacological data suggested that β-catenin signaling is altered by AgNP treatment *via* an indirect or complex mechanism (Cooper et al., 2019). Similarly, the pAkt signaling pathway is altered in cells exposed to AgNPs, but the mechanisms of AgNP interaction with this pathway are unclear (Spitzer et al., 2021). Neurite extension is critical during neurogenesis and depends on appropriate regulation of the F-actin and microtubule cytoskeleton (Valtorta and Leoni, 1999). The same cytoskeletal regulatory mechanisms are responsible for modulation of synaptic strength through growth and stabilization of dendritic spines on neurons; the structural underpinning for learning and memory throughout life (Hlushchenko et al., 2016). Therefore, it is important to understand how AgNPs interact with cellular mechanisms and alter physiological functions.

Here, we further investigate AgNP-induced dysregulation of cytoskeletal organization and examine localization of individual AgNPs in relation to the protein aggregates they induce. FAs are multi-protein links connecting intracellular actin to extracellular substrates, and they regulate numerous cell processes including differentiation, proliferation, and migration (Gilmore and Romer, 1996; Kawauchi, 2012). FA formation increases neurite outgrowth (Fischer et al., 2019) and is regulated by β-catenin signaling (Yu and Malenka, 2003); FAs may therefore, be a mechanistic target for AgNP-mediated cytoskeletal dysregulation. We used the rat B35 neuroblastoma cell line, an established model for examining mechanisms underlying neurite extension (Otey et al., 2003), to assess FA protein expression and organization in response to AgNP exposure. While not a direct substitute for cells in a living brain, immortalized cell lines utilize the same basic physiological and regulatory mechanisms and thereby provide useful functional insights. The B35 cell line is also easily maintained and differentiated without the need for growth factors, thus providing reproducible results over long time frames. Furthermore, using combined hyperspectral and fluorescence microscopy, we investigated the spatial relationship between individual AgNPs and protein aggregates. On a technical note, we determined the advantages of providing laminin as as an extracellular matrix to B35 cells in addition to the traditional poly-L-lysine (poly-K) and characterized the changes in hyperspectral properties of AgNP through cell culture and immunocytochemistry processing. This work will help clarify the underlying mechanisms that mediate cytoskeletal disruption induced by AgNP exposure and inform studies in more complex models. Further, it will aid in expanding awareness of brain health risks associated with low-level environmental AgNP exposure.

2. Methods

2.1. Nanoparticle characterization and preparation

AgNPs (40 nm) were purchased as a citrate-stabilized 20 μg/ml suspension (#730807; Sigma, St. Louis, MO). For characterization, AgNPs were dried on coverslips and coated with atomic carbon for scanning electron microscopy (SEM; JEOL, Peabody, MA). For energy dispersive spectroscopy (EDS) with the Ultim Max attachment from Oxford Instruments they were directly applied to a pure carbon mount (SPI Supplies, West Chester, PA). EDS Spectra were collected, and elemental peaks identified using AztecLive Spectrum acquisition and X-Ray smart mapping software. Spectra were collected with an emission of 20.0 Kev at a working distance of 10.0 mm. The diameter of individual particles was measured using ImageJ (NIH, Bethesda, MD). According to the manufacturer, the suspension is stable for 6 months. We therefore performed Dynamic Light Scattering analysis to confirm particle size when opening a new container and at 6 months or when the container was empty, whichever came first.

2.2. Cell culture and AgNP sample preparation

B35 neuroblastoma cells (CRL2754; ATCC, VA) were maintained adherent and undifferentiated in tissue culture (TC) flasks in complete medium containing 10% fetal bovine serum (FBS) in Dulbecco's Modified Eagle Medium (DMEM; Invitrogen, Carlsbad, CA) and 1% penicillin-streptomycin (P/S; Invitrogen). Medium was replaced every 2–3 days and cells were routinely passaged by trypsinization before reaching confluence. Glass coverslips (Fisher, Pittsburgh, PA) were coated with Poly-L-Lysine (poly-K; 0.01%; Sigma, St. Louis, MO) and laminin (1 μg/coverslip; Invitrogen) when indicated. Coated coverslips were placed in a 24-well plate. For experimentation, cells (passage 3–13) were washed with phosphate buffered saline (PBS1) (2.7 mM Na_2HPO_4 and 9.2 mM NaH_2PO_4 with PO_4 concentration 11.9 mM, 137 mM NaCl, 27 mM KCl, pH 7.4), trypsinized, and plated at 5×10^3 - 4×10^4 cells per well in differentiation medium (DMEM, 1% P/S) without FBS to promote differentiation. Cells differentiated for 1–3 days at 37 °C and 5% CO_2. After differentiation, half of medium was removed and replaced with fresh medium containing AgNPs (20 μg/ml stabilized in 2 mM citrate, 40 nm, such that the final AgNP concentration in each well was: 0 (negative control), 0.25, 0.50, 1.0, 2.0, or 4.0 μg/ml AgNPs). 2 mM citrate, a vehicle control, was added in matching doses so that each well contained the same amount of citrate.

A commercial Live/Dead assay (Thermo) was used to confirm cell viability in the AgNP treatments applied in this study. For this assay, B35 cells were maintained, differetiated on poly-K, and treated with 0 (negative control), 0.50, 1.0, 2.0, or 4.0 μg/ml AgNPs with 2 mM citrate, a vehicle control, to balance the volume as described above. Cells were washed thrice with PBS1 and then stained for 30 min 37 °C and 5% CO_2 with a freshly made working solution of PBS1 containing 2 μM each ethidium homodimer-1 and calcein-AM. Coverslips were then mounted on glass slides with PBS1 and images were immediately collected. To provide a positive control for the dead label, coverslips with differentiated but otherwise untreated cells were incubated with 70% methanol in PBS1 for 30 min 37 °C and 5% CO_2 after the first wash and then labeled with working solution and mounted for imaging as above.

To investigate changes in hyperspectral properties of citrate-stabilized AgNP, the commercially sourced 20 μg/ml AgNP suspension was mounted directly and imaged immediately or mounted in Prolong Gold and allowed to cure as above. We also applied AgNPs to coated coverslips in the absence of cells and incubated (37 °C and 5% CO_2) overnight in PBS1, in differentiation medium, or in differentiation medium followed by immunocytochemistry processing through to the end of the block step as described above. AgNPs on coverslips were mounted in Prolong Gold and cured as above.

2.3. Immunocytochemistry processing

Cells were washed with PBS1 and fixed in fresh 4% paraformaldehyde (Fisher) in PBS1 for 15 min followed by washing with PBS2 (20 mM NaH_2PO_4, 80 mM Na_2HPO_4, 152 mM NaCl, pH 7.4) and permeabilization with 0.3% Triton-X/PBS2 for 10 min. Blocking solution of 5% bovine serum albumin (BSA; Fisher) and 10% normal goat serum (NGS; Invitrogen) was applied for one hour. Primary antibodies to label intracellular proteins were then applied overnight at 4 °C. Antibodies were rabbit-α-vinculin (#MA5–11690; Invitrogen) or rabbit-

α-pan-cadherin (#717100; Invitrogen) at 1:250 in block solution. Coverslips were washed with PBS2, and secondary antibody goat-α-rabbit Alexa 488 (Invitrogen) was applied (1:500 in PBS2) for two hours. Coverslips were washed again with PBS2, and phalloidin Alexa 568, an F-actin cytoskeletal label, was added in PBS2 at 1:100 dilution for 20 min at room temperature. Cells were then washed and stained with 1 μg/ml DAPI (4′,6-diamidino-2-phenylindole; Sigma), a DNA marker, for 5 min. Coverslips were gently washed with Milli-Q water and mounted with Prolong Gold. Slides cured at room temperature overnight and were then stored at −20 °C.

2.4. Immunoblot analysis

B35 cells were plated as above and differentiated for 2–3 days in 6-well TC-coated plates with differentiation medium as previously described. AgNPs were added to half of the wells to 1 μg/ml 24 h before collection, and 2 mM citrate was added to the remaining wells as a vehicle control. Cells were washed with PBS1, trypsinized, and collected by centrifugation. Cells were suspended in SDS-PAGE buffer (Cell Signaling Technology (CST), Danvers, MA), sonicated for 15 s, and heated at 95 °C for 10 min. Samples were chilled on ice and stored at −80 °C. Protein samples were separated by gel electrophoresis on TGX stain-free acrylamide gels and transferred to a polyvinylidene fluoride (PVDF) membrane (GVS, Sanford, ME). Total protein content was imaged before and after transfer to PVDF as visualized with the TGX stain-free system. Blocking solution with 4% skim milk powder in Tween-Tris buffered saline (TTBS; 20 mM Tris, 500 mM NaCl, pH 7.5 plus 0.1% Tween20) was added to blots for 1 h minimum, then washed with TTBS before incubation. Blots were incubated overnight at 4 °C with rabbit-α-vinculin (1:500) in 5% BSA in TTBS, then washed five times in TTBS, and incubated with HRP-conjugated goat α-rabbit secondary antibody (1:2000; CST) for 1 h in BSA and TTBS. Blots were washed five times in TTBS and developed with chemiluminescent detection reagent (Thermo, Rockford, IL). Images of chemiluminescent signal were obtained using ChemiDoc XRS+ Imaging System (BioRad, Hercules, CA), and each band was normalized to total protein in that lane obtained *via* the TGX stain. Samples were run in triplicate and the mean band intensity was calculated and AgNP was normalized to citrate control for each experiment.

2.5. Image acquisition and analysis

A Leica inverted epifluorescent microscope with automated stage was used to collect fluorescent image mosaics from the center of each coverslip for the live/dead assay. An equally-sized area (~1.8 × 1.8 mm) was then cropped from each image and the number of live and dead cells were counted manually with the multi-point tool in ImageJ (NIH). The mean number of cells counted from each coverslip was 456. The proportion of live cells was calculated as a percent of the total number of cells.

Fluorescent images for analysis of vinculin label intensity and cadherin aggregate formation were obtained with a Leica inverted epiflourescent microscope. Images of AgNPs were collected with a Cytoviva Hyperspectral System (CytoViva, Auburn, AL) which allows acquisition of hyperspectral and fluorescence images from the same field of view. We used 60× and 100× lenses and exposure times of 0.05–0.25 s.

For quantitative assessment of cadherin and vinculin labels in immunocytochemistry experiments, epifluorescent RGB images of phalloidin, cadherin/vinculin, and DAPI were merged in ImageJ to provide clear neurite and nuclei structures. Images were converted to 8-bit and total neurite length per cell was measured using the the NeuronJ plugin (Meijering et al., 2004). ImageJ was used to measure fluorescence intensity in epifluorescent images as follows: Greyscale images (8-bit) of phalloidin were thresholded to include full cell bodies, and regions of interest (ROI) were defined for thresholded neurons (2 or more neurites longer than cell body) excluding binucleated or dead cells (small, rounded cells with minimal outgrowth and DAPI fluorescence). This ROI was applied to the corresponding 8-bit greyscale cadherin or vinculin channel, and area, mean particle intensity, and integrated density were measured and recorded. Integrated density measurements equaled the product of cell area and mean gray intensity, this allowed protein expression to be quantified without influence of cell size or number of cells measured per image.

For analysis of cadherin aggregate formation, RGB images of phalloidin, pan-cadherin, and DAPI were used. The green channel, labeling pan-cadherin, was thresholded to a different value per experiment determined using control images to clearly show aggregates. ImageJ cell counter was used to count total neurons following the same neuron characterizing standards as above. Neurons expressing small, bright cadherin aggregates were counted, and the number of neurons with aggregates were calculated as a proportion of the total number of neurons in each experimental group. Neurons expressing multiple cadherin aggregations were counted once. Cell counts were expressed as percent of total number of neurons.

Hyperspectral images were obtained from stock AgNP suspensions and from AgNPs applied to coverslips and processed through different stages of cell culture and immunocytochemistry processing as specified. Spectra for individual nanoparticles were obtained. In preparations with cells, fluorescent images were collected first followed by hyperspectral imaging of the identical field of view.

3. Results

3.1. AgNP characterization

SEM of commercially sourced citrate-stabilized AgNPs confirms that individual particles were spherical (Fig. 1A) with an average diameter of 44 nm (Fig. 1B). The purity of the nanoparticles was confirmed by a strong silver spectral signature localized to individual nanoparticles in EDS analysis (Fig. 1C-F).

3.2. AgNP treatments are sub-lethal and laminin promotes neurite extension in differentiating B35 neuroblastoma cells

A live/dead assay confirmed that AgNP treatment up to 4 μg/ml did not alter the proportion of live cells in the culture (Fig. 2A). We treated one set of differentitated cells with 70% methanol to provide a positive control for the dead label and found 100% dead cells on these coverslips (data not shown).

Cells plated on laminin-coated coverslips extended significantly longer neurites than cells plated on only poly-K (Fig. 2). Mean neurite length for cells on poly-K only was 35.4 μm, whereas cells on poly-K plus laminin consistently extended neurites averaging 75.9 μm (Fig. 2B). Moreover, maximum neurite length increased similarly to average neurite length in cells on laminin. In all experiments, neurons plated on laminin extended numerous long neurites with extensive branching. The longest neurite on each neuron was approximately 95.2 μm, nearly double that of poly-K only with an average 43.7 μm longest neurite (Fig. 2C). Qualitatively, cells on laminin were more likely to extend two or three neurites, compared to many unipolar cells observed on poly-K alone, and had more lamellipodia. However, the disruptive effect of AgNP on neurite length was unchanged in cells grown on laminin; the maximum neurite length collapsed to an average 63.3% of citrate control in cells exposed to 1 μg/ml AgNP (Fig. 2D). Lamellipodia formation also appeared to decrease in AgNP exposed cells.

3.3. Dose-dependent formation of cadherin aggregates in cells exposed to AgNPs colocalize with F-actin inclusions, but vinculin expression is unchanged

Cadherin formed small aggregates in the neurites of differentiating B35 cells with and without exposure to AgNPs, with aggregates often

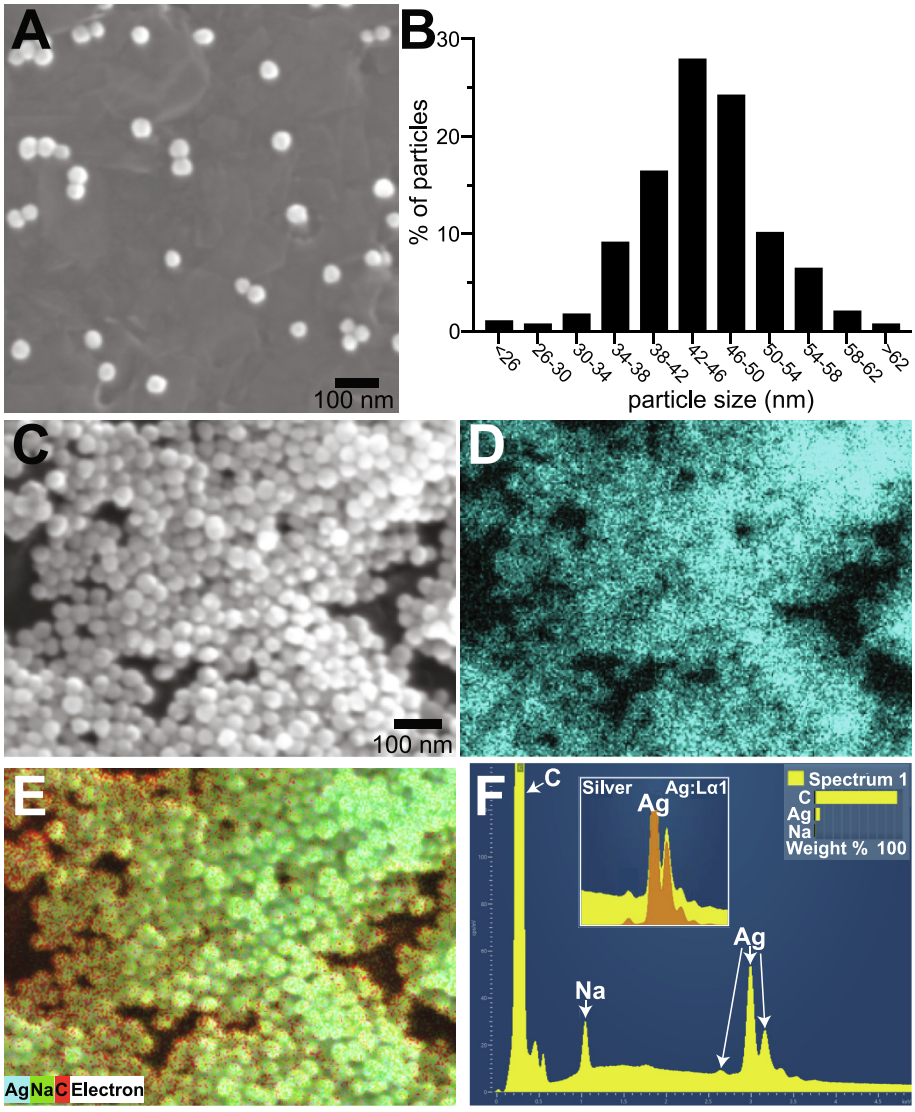

Fig. 1. Characterization of citrate-stabilized nanoparticle suspension. A) SEM performed 5.5 months after opening and storage at 4 °C confirms uniform size and shape. B) Size distribution of nanoparticles as measured by SEM. Total 298 particles measured. C) SEM of a mass of AgNPs used for D) EDS analysis to confirm pure Ag particles. E) overlay of SEM and EDS images. F) EDS spectrum confirms the presence of only Ag by comparison to reference spectrum (inset, orange) plus C and Na from citrate.

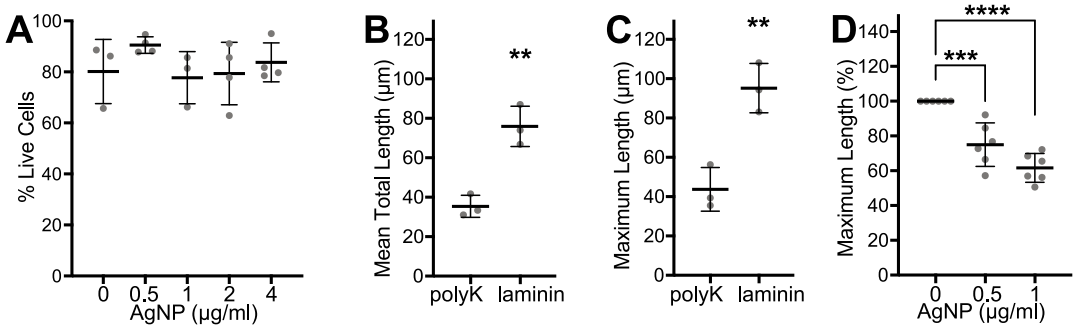

Fig. 2. Viability is not inhibited by the doses of AgNP applied here. Laminin increases neurite outgrowth in the B35 cell line *in vitro* but does not alter AgNP-induced neurite collapse. A) The proportion of live cells in the culture after 24 h of incubation in 0–4 μg/ml AgNPs is unchanged. $N = 3$–4 independent experiments. One-way ANOVA $p > 0.05$. B) Mean total neurite length and C) Maximum neurite length of B35 cells are increased when cells are plated on poly-K plus laminin, compared to poly-K alone. Unpaired two-tailed *t*-test, ** $p < 0.01$. D) Cells grown on poly-K and laminin exhibit neurite collapse in response to AgNP. $N = 6$ independent experiments and 45–95 cells analyzed per experiment. One-way ANOVA followed by Dunnett's multiple comparisons; ***$p < 0.001$; ****$p < 0.0001$; values presented as % of control. Lines and errors indicate mean ± SD for A-D.

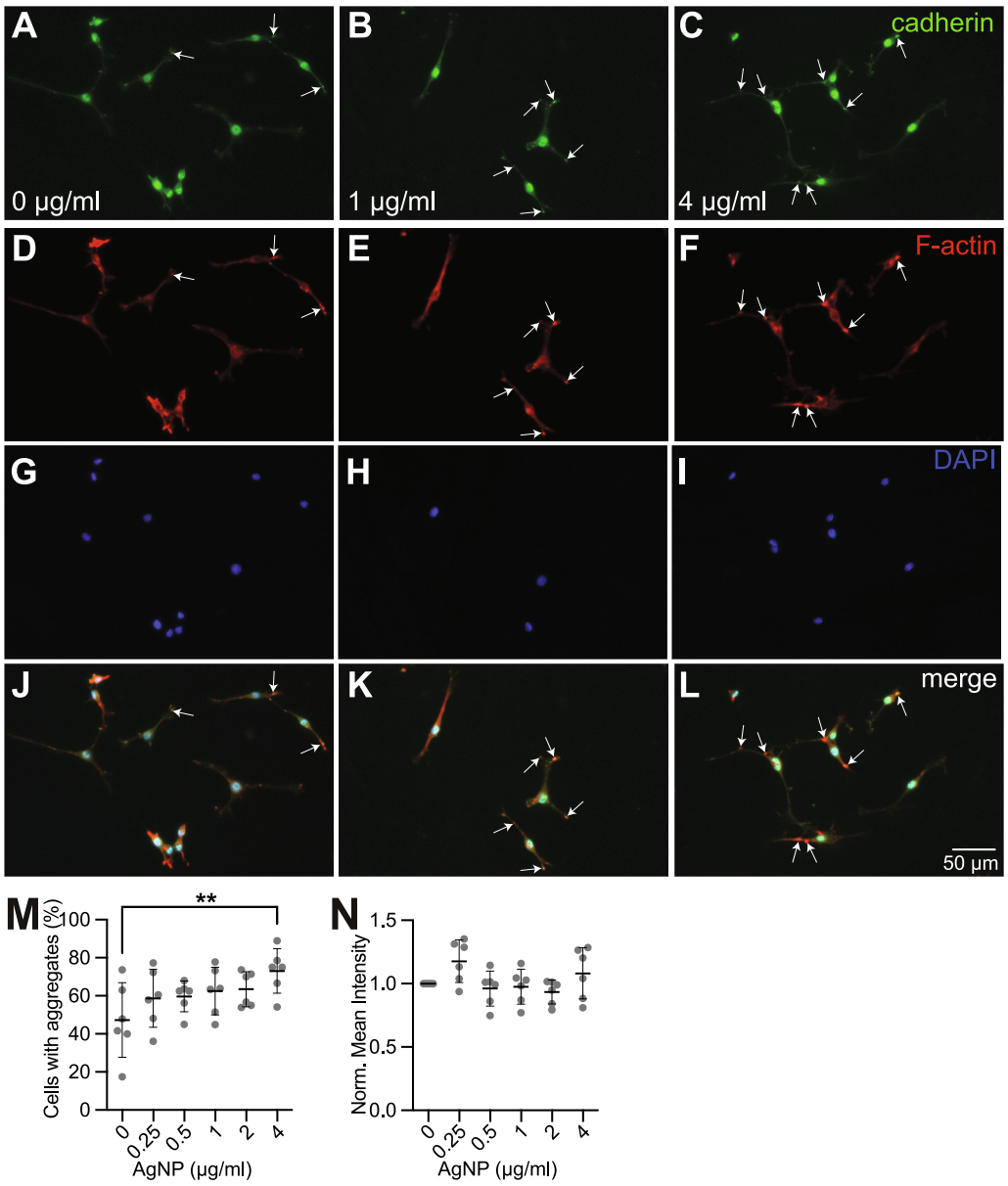

Fig. 3. AgNP exposure induces formation of cadherin protein aggregates that colocalize with F-actin inclusions in cultured differentiating B35 cells. Cadherin aggregates (arrows) are visible in cells treated with A) Citrate control; B) 1 µg/ml AgNPs; C) 4 µg/ml AgNPs. D—F) AgNPs also induce formation of F-actin inclusions. G-I) Nuclei are stained blue with DAPI. J-L) Merged images demonstrate that cadherin aggregates tend to colocalize with f-actin inclusions. Green: pan-cadherin, Red: F-actin, Blue: DAPI (nuclei). M) Summary data from $N = 6$ independent experiments show a dose-dependent increase in cadherin aggregate formation. Mean + SD, one-way ANOVA followed by Sidak's multiple comparisons. $^{**}p < 0.01$. N) The cadherin label intensity did not change with AgNP treatment. One-way ANOVA. $p > 0.05$. (For interpretation of the references to colour in this figure legend, the reader is referred to the web version of this article.)

forming near neurite endings (Fig. 3A-C). As we reported previously (Cooper and Spitzer, 2015) AgNPs also induced F-actin inclusions (Fig. 3D-F) and these colocalize with β-catenin (Cooper et al., 2019). DAPI was used to stain nuclei (Fig. 3 G-I) and merged images confirm that cadherin aggregates also colocalize with F-actin inclusions (Fig. 3J-L). The proportion of cells with cadherin aggregates increased in a dose-dependent manner when cells were exposed to increasing AgNP concentrations; and approximately half the cells exhibited one or more aggregates in the control group, and this number increased to about 60% with 1 µg/ml AgNPs and nearly 80% in 4 µg/ml AgNPs (Fig. 3M). However, the total labeling intensity of cadherin in individual cells did not change significantly with AgNP exposure (Fig. 3N). Cultured differentiated B35 cells strongly expressed vinculin (Fig. 4A), however, the expression levels or organization of vinculin, did not change with AgNP exposure as measured by signal intensity in immunocytochemistry (Fig. 4B) or immunoblot (Fig. 4C) analysis.

3.4. *Hyperspectral properties of AgNPs become more uniform after immunocytochemical processing*

Commercially sourced AgNPs present as a rainbow assortment in hyperspectral microscopy, this spectral variability is retained when AgNPs are mounted in Prolong Gold (Fig. 5). AgNPs mounted in Prolong Gold (Fig. 5 A, B) mostly present spectra centered on blue (Fig. 5B_1) with some particles presenting rainbow colors (Fig. 5B_2, B_3). This variability is maintained when AgNPs are adhered to poly-K/laminin-coated coverslips, incubated in PBS2 and wet-mounted for immediate imaging. However, AgNP spectra collected from samples that were processed through cell culture conditions (Fig. 5D) or immunocytochemistry (Fig. 5E) presented uniform spectra that were shifted to center on green.

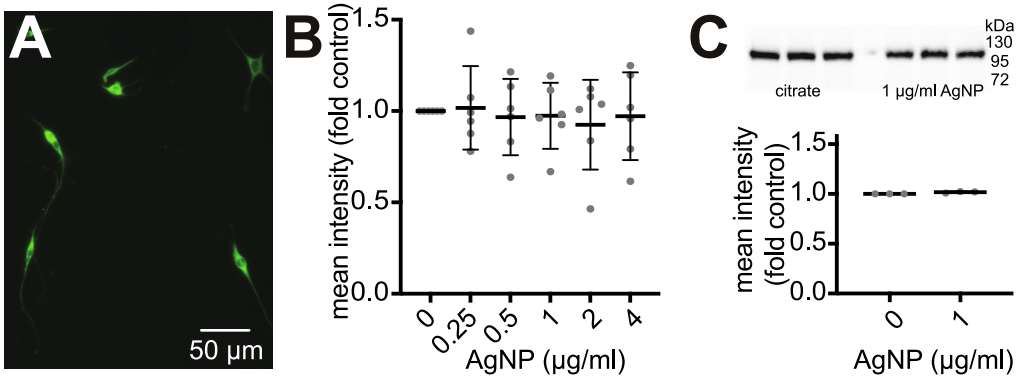

Fig. 4. Vinculin expression in B35 neuroblastoma cells following AgNP exposure. A) Vinculin immunofluorescence (green) in dose response control; B) Mean intensity of vinculin immunofluorescence does not change with increasing AgNP exposure. One-way ANOVA $p > 0.05$, $N = 6$ independent experiments. C) Representative vinculin immunoblot (top) and quantitative analysis of normalized band intensity indicate no change in vinculin expression with AgNP exposure. Independent *t*-test $p > 0.05$. $N = 3$ independent experiments with each sample run in triplicate.

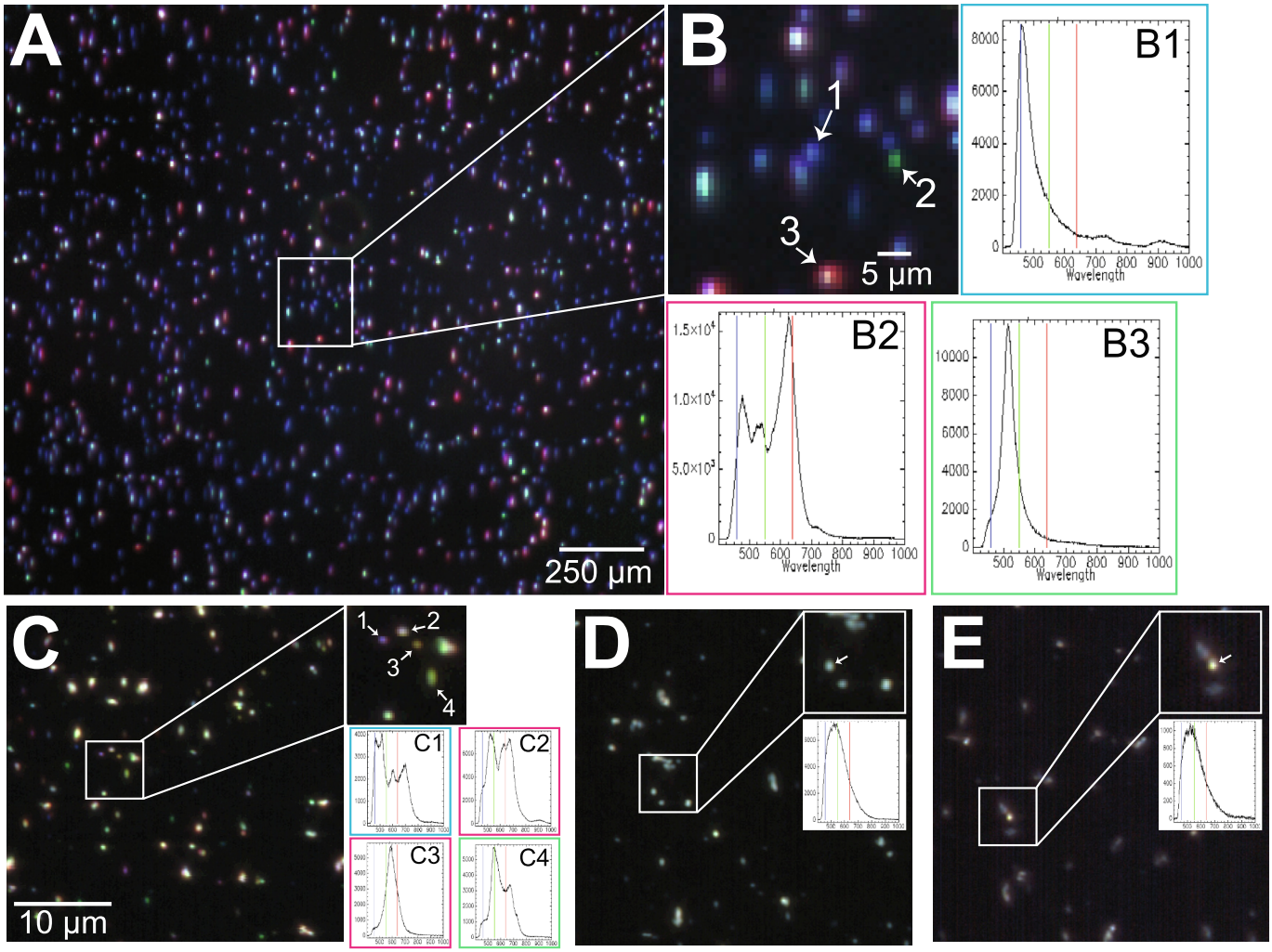

Fig. 5. Hyperspectral imaging of commercially purchased AgNPs A) mounted directly from stock solution. B) Higher magnification view of indicated area shows individual nanoparticles and their representative spectral properties. C) AgNPs adhered to poly-K/laminin-coated coverslips and incubated in PBS1. D) AgNPs adhered to coated coverslips and incubated in differentiation medium. E) as in D but processed though to block step of immunocytochemistry. For C-E, insets show higher magnification of indicated area and representative spectra for indicated individual nanoparticles. All preparations except C (wet-mounted) were mounted in Prolong Gold. (For interpretation of the references to colour in this figure legend, the reader is referred to the web version of this article.)

3.5. Protein aggregates induced by AgNPs do not colocalize with AgNPs themselves in neurites

Hyperspectral microscopy in combination with fluorescent imaging allowed visualization of individual AgNP (Fig. 6A) and cellular protein aggregates (Fig. 6B) in the same field of view and superimposed (Fig. 6C). AgNPs in cell preparations had the same green-shifted spectra regardless of whether they were associated with a cell (Fig. 6D_1) or free on the coverslip (Fig. 6D_2). We confirmed colocalization of cadherin aggregates and F-actin inclusions. The F-actin inclusions did not colocalize with AgNPs in the neurites, however colocalization may occur in the cytoplasmic and periuclear regions (Fig. 6E-I).

4. Discussion

AgNPs continue to be used as an antimicrobial in manufacturing healthcare products, textiles and many consumer goods. Nanoparticles are released into the environment resulting in widespread exposure of humans and wildlife. AgNPs can cross the blood-brain barrier and bioaccumulate in the brain causing neuronal damage (Recordati et al., 2021; Tang et al., 2010). We previously reported that AgNP exposure induces neurite collapse and leads to cytoskeletal dysregulation and formation of F-actin inclusions (Cooper and Spitzer, 2015). The regulatory protein β-catenin also aggregated in response to AgNP exposure and colocalized with F-actin inclusions (Cooper et al., 2019). Furthermore, we found that β-catenin and Akt intracellular signaling were indirectly disrupted by AgNP exposure in B35 neuroblastoma cells (Spitzer et al., 2021). However, specific physiological mechanisms mediating these effects are not well understood. Here, we investigated the expression and organization of the FA proteins cadherin and vinculin in B35 cell exposed to AgNPs, and we utilized hyperspectral microscopy to determine if AgNP-induced protein aggregates colocalize with AgNPs in cells.

Laminin is the primary component of extracellular matrices in mammals and is generally coated on substrates for neural cell culture (Fudge and Mearow, 2013; Domogatskaya et al., 2012). However, the B35 cell line is routinely differentiated only on poly-K or tissue culture-coated plastic (Otey et al., 2003). Laminin specifically triggers neurite outgrowth processes in the cell (McKerracher et al., 1996) through interactions with vinculin and it is traditionally used for *in vitro* neuronal differentiation in many cell lines because it mimics the *in vivo* extracellular environment. For example, laminin promotes differentiation in

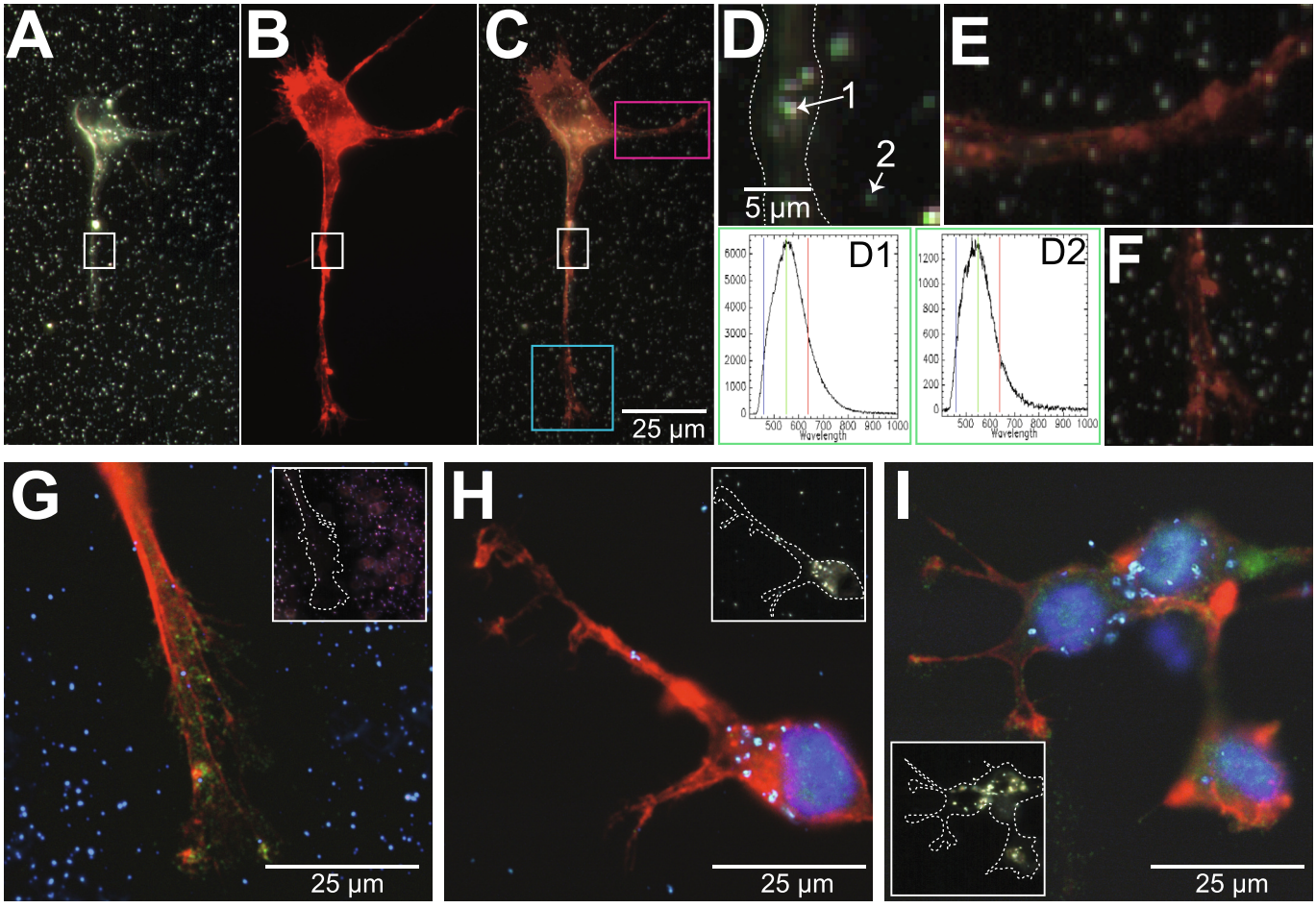

Fig. 6. Hyperspectral imaging of AgNP-exposed cells shows that protein aggregates do not colocalize with nanoparticles. A) Hyperspectral imaging of a B35 cell exposed to AgNPs B) fluorescence imaging of the same field of view delineates F-actin labeled with phalloidin-Alexa 568 in the same cell and C) an overlay of hyperspectral and fluorescence images allows localization of AgNPs in relation to F-actin structures. D) Higher magnification of indicated area from the hyperspectral image (white box) shows that spectra presented by AgNPs are centered on green regardless of their localization with cells (D1) or alone (D2). Dotted lines in D indicate outline of the cell's neurite. E) Higher magnification of areas from the hyperspectral/fluorescence overlay indicated in E) magenta and F) cyan boxes show that nanoparticles associated with cells do not colocalize with F-actin inclusions. G-I) Cells from other experiments confirm that AgNPs (visualized by darkfield microscopy) do not colocalize with F-actin (red) and cadherin (green) aggregates. Nuclei are stained blue with DAPI. Insets in G-I show hyperspectral image for same field of view with dotted lines indicating outline of cell. (For interpretation of the references to colour in this figure legend, the reader is referred to the web version of this article.)

cultured neural tube neurons (Heaton and Swanson, 1988), human sensory neurons (Baron-Van Evercooren et al., 1982), and human embryonic stem cells (Ma et al., 2008). Despite the extensive use of laminin in other cell lines, B35 cells are traditionally not provided this substrate (Otey et al., 2003). We found that, although B35 cells will adhere and extend branched neurites on only poly-K, they do so much more effectively when provided laminin. Laminin also promoted multipolar neurite extension, representative of neurons that play a critical role in central and peripheral nervous system function (Ludwig et al., 2023), and development of lamellipodia which form growth cones that guide neurite development (Clark et al., 1993). Thus, providing laminin to the B35 cell line during differentiation appears to promote morphological differentiation and may provide a more representative model system for evaluating mechanisms of neurite extension.

The neurite collapse we previously reported in cultured adult neural stem cells and in B35 cells grown on poly-K (Cooper and Spitzer, 2015) exposed to 1 μg/ml AgNPs was still evident in B35 cells plated on laminin. Neurite outgrowth occurs during neurogenesis, a process required for learning, memory formation, and overall brain development (van Praag et al., 1999). Because AgNP-induced defects also occur in the presence of laminin in the B35 cell line, and laminin is more representative of the *in vivo* environment, these data support previous findings and indicate that AgNP exposure may disrupt nervous system development. This is especially relevant to children who may be exposed to many sources of environmental AgNPs (Quadros et al., 2013) and, given the tendency of AgNP to bioaccumulate in brain (Recordati et al., 2021; Lee et al., 2013; Tang et al., 2008; van der Zande et al., 2012; Skalska et al., 2015; Skalska et al., 2020; Antsiferova et al., 2021), may face years of low-level exposure. Although tissues such as liver are thought to compensate for damage from locally accumulated AgNPs (Quadros et al., 2013), brain tissue is organized differently and much more specifically; one brain structure may not readily be able to compensate for chronic damage at another circuit or collection of synapses.

Cadherins mediate several pathways important to neuronal differentiation and development including Rho GTPases (Derycke and Bracke, 2004). N-cadherin, which is specific to neurons, can mediate neuron outgrowth through interaction with vinculin and other proteins at focal adhesions (Mui et al., 2016). We found that cadherin formed more intracellular cadherin aggregates in response to increasing exposure to AgNPs in differentiating B35 cells. In cultured primary human keratinocytes, AgNP exposure increased E-cadherin localization to cell-cell junctions and increased cell motility (Montano et al., 2019), suggesting that E-cadherin may be reorganizing in a directed manner. Similarly, we found that cadherin aggregates frequently colocalized with the F-actin inclusions elicited by AgNP exposure in B35 cells. We previously reported these inclusions to colocalize also with β-catenin (Cooper et al., 2019). During normal differentiation, N-cadherin directly interacts with actin and β-catenin (Seong et al., 2015). These data therefore suggest that AgNPs are inducing specific reorganizational mechanisms of cytoskeletal and associated proteins to generate multi-protein aggregates in response to AgNP exposure. This interpretation is supported by the lack of localization of vinculin to aggregates in response to AgNP. If the aggregates were nonspecific agglomerations of cytoskeletal and associated proteins in the neurite, they would be expected to include vinculin. Vinculin is a FA protein that regulates neurite extension (Goldmann et al., 2013; Mierke et al., 2010). It is widely expressed in cultured B35 cells and normally engages in direct interactions with cadherin, β-catenin, and actin (Bays et al., 2014), but its expression levels did not change with AgNP exposure and it was not observed to aggregate.

Hyperspectral microscopy is a powerful tool to visualize nanomaterials and examine their physical properties. We used this technique to demonstrate that the hyperspectral signal of individual particles in a commercial citrate-stabilized AgNP solution is variable. Many particles exhibited a spectrum centered on blue, as expected from pure, freshly suspended AgNPs, but some presented rainbow colors that occur due to red-shifting of the resonance peak when nanoparticles aggregate (CytoViva, 2022). Accordingly, SEM analysis confirmed a small proportion of particles that appeared to be aggregated in pairs or triplets (Fig. 1). However, hyperspectral and SEM imaging indicate that most particles are unaggregated. We found that AgNPs exposed to cell culture conditions presented a spectrum that was shifted to center on green with a loss of the variability seen in particles from the stock solution. The blue/rainbow spectra were still evident after AgNPs were plated on poly-K/laminin coverslips and incubated in PBS, and the green shift only occurred when particles were incubated in cell culture medium. Processing through immunohistochemistry did not further alter the green-centered spectral signal from the AgNPs. This suggests that it is the complex organic molecules such as amino acids and vitamins from the cell culture medium, which does not contain proteins, that are responsible for the consistent green spectral shift. Further addition of proteins with the blocking step of immunocytochemistry processing likely induces formation of a corona, but does not further alter the particles' hyperspectral properties. Furthermore, there was no difference in the spectra presented by AgNPs on the coverslip and those associated with cells in immunocytochemistry preparations, suggesting that any additional cellular proteins that associate with the AgNPs do not impact hyperspectral properties. Unlike AgNPs that were actively taken up and sequestered in lysosomes by macrophage (Shannahan et al., 2015), we did not find a significant red shift in the spectra of AgNPs associated with B35 cells; their spectra remained centered on green around 550 nm regardless of whether they were on or beside cells. This further suggests that neural cells do not use protein aggregate structures to generate AgNP clusters which would be expected to generate interactions between the particles' charge density oscillations resulting in a further red shift (Shannahan et al., 2015).

In biological conditions AgNPs release ionic Ag; this is generally accepted to be a source of toxic effects of AgNPs. AgNPs acquire protein coronas that stabilize them and change their physical properties and their interactions with biological mechanisms (Miclaus et al., 2014). This protein coat may provide purchase for cellular protective mechanisms that attempt to sequester the AgNPs within proteinacous structures to minimize Ag release and associated cellular damage. However, we found that the multi-protein aggregates formed by exposure to AgNPs do not colocalize with the AgNPs themselves and are therefore not likely to represent such a sequestration mechanism. Furthermore, this separation of protein aggregates and AgNPs suggests that the aggregations are induced indirectly by cellular mechanisms that are in turn activated by the presence of AgNPs or the ionic Ag released from them. One such mechanism could be oxidative stress which is induced by AgNP in many cell types, including neural cells (Hadrup et al., 2012; Yin et al., 2013; Struzynski et al., 2014), and in animals (Struzynski et al., 2014; Wu and Zhou, 2012; Skalska et al., 2016; Dabrowska-Bouta et al., 2019). Indeed, redox signaling through physiologically appropriate levels of ROS is critical in regulating cytoskeletal dynamics (Wilson and Gonzalez-Billault, 2015).

Oxidative stress mechanisms activated by AgNPs can induce misfolding of cellular proteins, notably cytoskeletal proteins, that are then sequestered within aggresomes (Castro et al., 2017; Hackett et al., 2015; Rohde et al., 2021). These perinuclear microtubule-dependent inclusion bodies can include F-actin (Lazaro-Dieguez et al., 2008) and are formed by the cell when its capacity to degrade misfolded proteins is exceeded (Johnston et al., 1998; Kopito, 2000; Lazaro-Dieguez et al., 2008). Because N-cadherin directly interacts with actin and β-catenin during normal differentiation (Seong et al., 2015), it is not unexpected that these proteins might be processed together when internalized. Further, β-catenin marked for degradation accumulates in aggresomes in Alzheimer's disease, presumably due to proteasome dysfunction (Ghanevati and Miller, 2005). Therefore, AgNPs could promote misfolding of specific cellular proteins to a level that overwhelms degradation mechanisms, thereby leading to formation of aggresomes that contain F-actin, β-catenin, and cadherin. If this proposed mechanism is active in response to AgNPs, and because aggresomes form in the perinuclear region,

colocalization of protein aggregates and AgNPs is expected only in this region but not in the neurites. If AgNPs do induce aggresome formation, it will also be interesting to determine if protein aggregates formed in the neurites are transported to the soma for sequestration in aggresomes, if they are degraded in place, or if they accumulate over time.

In summary, AgNP exposure disrupts organization of the FA protein cadherin, which may contribute to neurite collapse. Cadherin colocalizes with F-actin inclusions along with β-catenin in response to AgNP exposure. These multi-protein aggregates do not include the FA protein vinculin or colocalize with AgNPs themselves, suggesting that they may be the result of specific protein-protein interactions that occur in response to regulatory signals induced by AgNPs. It is possible that AgNPs localized to the perinuclear region promote protein misfolding and formation of aggresomes. Identification of the specific mechanisms and interactions between these cellular components in response to AgNPs will help to understand the potential physiological effect of bioaccumulated AgNPs in brain tissue. This will aid in expanding awareness of brain health risks associated with environmental AgNP exposure and perhaps encourage manufacturers to consider other antimicrobial options.

CRediT authorship contribution statement

Kaden M. Thomas: Writing – review & editing, Writing – original draft, Methodology, Investigation, Formal analysis. **Nadja Spitzer:** Writing – review & editing, Writing – original draft, Validation, Supervision, Resources, Project administration, Methodology, Investigation, Funding acquisition, Formal analysis, Conceptualization.

Declaration of competing interest

The authors declare that they have no known competing financial interests or personal relationships that could have appeared to influence the work reported in this paper.

Data availability

Data will be made available on request.

Acknowledgements

This work was supported by National Science Foundation (NSF) award #1553667 to NS. Hyperspectral microscopy was performed on an instrument supported by NSF #2116140. KT was awarded a National Aeronautics and Space Administration West Virginia Space Grant Consortium Fellowship and a West Virginia Higher Education Policy Commission Division of Science and Research Grant Summer Undergraduate Research Experience Fellowship #dsr.20.16. We appreciate help in processing and imaging of cell preps by Nicole Rueff. We thank Dr. Rosalynn Quiñones of the Chemistry Department at Marshall University for Dynamic Light Scattering analysis. Scanning Electron Microscopy and Energy-dispersive X-ray Spectroscopy analysis was performed on an instrument supported by NSF #CHE1828358 at the Marshall University Molecular and Biological Imaging Center by Will Crockett with training and help from David Neff.

References

Antsiferova, A.A., Kopaeva, M.Y., Kochkin, V.N., Kashkarov, P.K., 2021. Kinetics of silver accumulation in tissues of laboratory mice after long-term oral administration of silver nanoparticles. Nanomaterials (Basel) 11 (12).

Baron-Van Evercooren, A., Kleinman, H.K., Ohno, S., Marangos, P., Schwartz, J.P., Dubois-Dalcq, M.E., 1982. Nerve growth factor, laminin, and fibronectin promote neurite growth in human fetal sensory ganglia cultures. J. Neurosci. Res. 8 (2–3), 179–193.

Bays, J.L., Peng, X., Tolbert, C.E., Guilluy, C., Angell, A.E., Pan, Y., Superfine, R., Burridge, K., DeMali, K.A., 2014. Vinculin phosphorylation differentially regulates mechanotransduction at cell-cell and cell-matrix adhesions. J. Cell Biol. 205 (2), 251–263.

Castro, J.P., Jung, T., Grune, T., Siems, W., 2017. 4-Hydroxynonenal (HNE) modified proteins in metabolic diseases. Free Radic. Biol. Med. 111, 309–315.

Clark, P., Britland, S., Connolly, P., 1993. Growth cone guidance and neuron morphology on micropatterned laminin surfaces. J. Cell Sci. 105 (Pt 1), 203–212.

Colman, B.P., Baker, L.F., King, R.S., Matson, C.W., Unrine, J.M., Marinakos, S.M., Gorka, D.E., Bernhardt, E.S., 2018. Dosing, not the dose: comparing chronic and pulsed silver nanoparticle exposures. Environ. Sci. Technol. 52 (17), 10048–10056.

Cooper, R.J., Spitzer, N., 2015. Silver nanoparticles at sublethal concentrations disrupt cytoskeleton and neurite dynamics in cultured adult neural stem cells. Neurotoxicology 48, 231–238.

Cooper, R.J., Menking-Colby, M.N., Humphrey, K.A., Victory, J.H., Kipps, D.W., Spitzer, N., 2019. Involvement of beta-catenin in cytoskeleton disruption following adult neural stem cell exposure to low-level silver nanoparticles. Neurotoxicology 71, 102–112.

CytoViva, 2022. Differentiating aggregating and dispersed silver nanoparticles. Accessed 10/14/2022. Available from: https://www.cytoviva.com/_files/ugd/338c3a_0c1d5fc0ab0c436ebd7e008fa7285d9a.pdf.

Dabrowska-Bouta, B., Sulkowski, G., Struzynski, W., Struzynska, L., 2019. Prolonged exposure to silver nanoparticles results in oxidative stress in cerebral myelin. Neurotox. Res. 35 (3), 495–504.

Derycke, L.D., Bracke, M.E., 2004. N-cadherin in the spotlight of cell-cell adhesion, differentiation, embryogenesis, invasion and signalling. Int. J. Dev. Biol. 48 (5–6), 463–476.

Domogatskaya, A., Rodin, S., Tryggvason, K., 2012. Functional diversity of laminins. Annu. Rev. Cell Dev. Biol. 28, 523–553.

Fabrega, J., Luoma, S.N., Tyler, C.R., Galloway, T.S., Lead, J.R., 2011. Silver nanoparticles: behaviour and effects in the aquatic environment. Environ. Int. 37 (2), 517–531.

Fischer, R.S., Lam, P.Y., Huttenlocher, A., Waterman, C.M., 2019. Filopodia and focal adhesions: an integrated system driving branching morphogenesis in neuronal pathfinding and angiogenesis. Dev. Biol. 451 (1), 86–95.

Fudge, N.J., Mearow, K.M., 2013. Extracellular matrix-associated gene expression in adult sensory neuron populations cultured on a laminin substrate. BMC Neurosci. 14, 15.

Ghanevati, M., Miller, C.A., 2005. Phospho-beta-catenin accumulation in Alzheimer's disease and in aggresomes attributable to proteasome dysfunction. J. Mol. Neurosci. 25 (1), 79–94.

Gilmore, A.P., Romer, L.H., 1996. Inhibition of focal adhesion kinase (FAK) signaling in focal adhesions decreases cell motility and proliferation. Mol. Biol. Cell 7 (8), 1209–1224.

Goldmann, W.H., Auernheimer, V., Thievessen, I., Fabry, B., 2013. Vinculin, cell mechanics and tumour cell invasion. Cell Biol. Int. 37 (5), 397–405.

Gottschalk, F., Sun, T., Nowack, B., 2013. Environmental concentrations of engineered nanomaterials: review of modeling and analytical studies. Environ. Pollut. 181, 287–300.

Guo, X., Zhang, G., Chen, L., Khan, A.A., Gu, B., Li, B., 2017. Newborn neurons are damaged in vitro by a low concentration of silver nanoparticles through the inflammatory oxidative stress pathway. DNA Cell Biol. 36 (12), 1062–1070.

Haase, A., Rott, S., Mantion, A., Graf, P., Plendl, J., Thunemann, A.F., Meier, W.P., Taubert, A., Luch, A., Reiser, G., 2012. Effects of silver nanoparticles on primary mixed neural cell cultures: uptake, oxidative stress and acute calcium responses. Toxicol. Sci. 126 (2), 457–468.

Hackett, M.J., Smith, S.E., Caine, S., Nichol, H., George, G.N., Pickering, I.J., Paterson, P. G., 2015. Novel bio-spectroscopic imaging reveals disturbed protein homeostasis and thiol redox with protein aggregation prior to hippocampal CA1 pyramidal neuron death induced by global brain ischemia in the rat. Free Radic. Biol. Med. 89, 806–818.

Hadrup, N., Loeschner, K., Mortensen, A., Sharma, A.K., Qvortrup, K., Larsen, E.H., Lam, H.R., 2012. The similar neurotoxic effects of nanoparticulate and ionic silver in vivo and in vitro. Neurotoxicology 33 (3), 416–423.

Heaton, M.B., Swanson, D.J., 1988. The influence of laminin on the initial differentiation of cultured neural tube neurons. J. Neurosci. Res. 19 (2), 212–218.

Hlushchenko, I., Koskinen, M., Hotulainen, P., 2016. Dendritic spine actin dynamics in neuronal maturation and synaptic plasticity. Cytoskeleton (Hoboken) 73 (9), 435–441.

Johnston, J.A., Ward, C.L., Kopito, R.R., 1998. Aggresomes: a cellular response to misfolded proteins. J. Cell Biol. 143 (7), 1883–1898.

Kakakhel, M.A., Wu, F., Sajjad, W., Zhang, Q., Khan, I., Ullah, K., Wang, W., 2021. Long-term exposure to high-concentration silver nanoparticles induced toxicity, fatality, bioaccumulation, and histological alteration in fish (Cyprinus carpio). Environ. Sci. Eur. 33 (1), 14.

Kawauchi, T., 2012. Cell adhesion and its endocytic regulation in cell migration during neural development and cancer metastasis. Int. J. Mol. Sci. 13 (4), 4564–4590.

Kopito, R.R., 2000. Aggresomes, inclusion bodies and protein aggregation. Trends Cell Biol. 10 (12), 524–530.

Lazaro-Dieguez, F., Aguado, C., Mato, E., Sanchez-Ruiz, Y., Esteban, I., Alberch, J., Knecht, E., Egea, G., 2008. Dynamics of an F-actin aggresome generated by the actin-stabilizing toxin jasplakinolide. J. Cell Sci. 121 (Pt 9), 1415–1425.

Lee, J.H., Kim, Y.S., Song, K.S., Ryu, H.R., Sung, J.H., Park, J.D., Park, H.M., Song, N.W., Shin, B.S., Marshak, D., Ahn, K., Lee, J.E., Yu, I.J., 2013. Biopersistence of silver nanoparticles in tissues from Sprague-Dawley rats. Part. Fibre Toxicol. 10, 36.

Lee, S.H., Ko, H.M., Kwon, K.J., Lee, J., Han, S.H., Han, D.W., Cheong, J.H., Ryu, J.H., Shin, C.Y., 2014. tPA regulates neurite outgrowth by phosphorylation of LRP5/6 in neural progenitor cells. Mol. Neurobiol. 49 (1), 199–215.

Liu, F., Mahmood, M., Xu, Y., Watanabe, F., Biris, A.S., Hansen, D.K., Inselman, A., Casciano, D., Patterson, T.A., Paule, M.G., Slikker Jr., W., Wang, C., 2015. Effects of silver nanoparticles on human and rat embryonic neural stem cells. Front. Neurosci. 9, 115.
Ludwig, P.E., Reddy, V., Varacallo, M., 2023. Neuroanatomy, neurons. In: StatPearls. Treasure Island (FL) ineligible companies. Disclosure: Vamsi Reddy declares no relevant financial relationships with ineligible companies. Disclosure: Matthew Varacallo declares no relevant financial relationships with ineligible companies.
Ma, W., Tavakoli, T., Derby, E., Serebryakova, Y., Rao, M.S., Mattson, M.P., 2008. Cell-extracellular matrix interactions regulate neural differentiation of human embryonic stem cells. BMC Dev. Biol. 8, 90.
McGillicuddy, E., Murray, I., Kavanagh, S., Morrison, L., Fogarty, A., Cormican, M., Dockery, P., Prendergast, M., Rowan, N., Morris, D., 2017. Silver nanoparticles in the environment: sources, detection and ecotoxicology. Sci. Total Environ. 575, 231–246.
McKerracher, L., Chamoux, M., Arregui, C.O., 1996. Role of laminin and integrin interactions in growth cone guidance. Mol. Neurobiol. 12 (2), 95–116.
Meijering, E., Jacob, M., Sarria, J.C., Steiner, P., Hirling, H., Unser, M., 2004. Design and validation of a tool for neurite tracing and analysis in fluorescence microscopy images. Cytometry A 58 (2), 167–176.
Miclaus, T., Bochenkov, V.E., Ogaki, R., Howard, K.A., Sutherland, D.S., 2014. Spatial mapping and quantification of soft and hard protein coronas at silver nanocubes. Nano Lett. 14 (4), 2086–2093.
Mierke, C.T., Kollmannsberger, P., Zitterbart, D.P., Diez, G., Koch, T.M., Marg, S., Ziegler, W.H., Goldmann, W.H., Fabry, B., 2010. Vinculin facilitates cell invasion into three-dimensional collagen matrices. J. Biol. Chem. 285 (17), 13121–13130.
Montano, E., Vivo, M., Guarino, A.M., di Martino, O., Di Luccia, B., Calabrò, V., Caserta, S., Pollice, A., 2019. Colloidal silver induces cytoskeleton reorganization and E-cadherin recruitment at cell-cell contacts in HaCaT cells. Pharmaceuticals (Basel) 12 (2).
Mui, K.L., Chen, C.S., Assoian, R.K., 2016. The mechanical regulation of integrin-cadherin crosstalk organizes cells, signaling and forces. J. Cell Sci. 129 (6), 1093–1100.
Muller, P., Langenbach, A., Kaminski, A., Rychly, J., 2013. Modulating the actin cytoskeleton affects mechanically induced signal transduction and differentiation in mesenchymal stem cells. PloS One 8 (7), e71283.
Otey, C.A., Boukhelifa, M., Maness, P., 2003. B35 neuroblastoma cells: an easily transfected, cultured cell model of central nervous system neurons. Methods Cell Biol. 71, 287–304.
Quadros, M.E., Pierson, R., Tulve, N.S., Willis, R., Rogers, K., Thomas, T.A., Marr, L.C., 2013. Release of silver from nanotechnology-based consumer products for children. Environ. Sci. Technol. 47 (15), 8894–8901.
Recordati, C., De Maglie, M., Cella, C., Argentiere, S., Paltrinieri, S., Bianchessi, S., Losa, M., Fiordaliso, F., Corbelli, A., Milite, G., Aureli, F., D'Amato, M., Raggi, A., Cubadda, F., Soldati, S., Lenardi, C., Scanziani, E., 2021. Repeated oral administration of low doses of silver in mice: tissue distribution and effects on central nervous system. Part. Fibre Toxicol. 18 (1), 23.
Rohde, M.M., Snyder, C.M., Sloop, J., Solst, S.R., Donati, G.L., Spitz, D.R., Furdui, C.M., Singh, R., 2021. The mechanism of cell death induced by silver nanoparticles is distinct from silver cations. Part. Fibre Toxicol. 18 (1), 37.
Samberg, M.E., Monteiro-Riviere, N.A., 2014. Silver nanoparticles in biomedical applications. In: Nanotoxicology. CRC Press.
Seong, E., Yuan, L., Arikkath, J., 2015. Cadherins and catenins in dendrite and synapse morphogenesis. Cell Adh. Migr. 9 (3), 202–213.
Shannahan, J.H., Podila, R., Brown, J.M., 2015. A hyperspectral and toxicological analysis of protein corona impact on silver nanoparticle properties, intracellular modifications, and macrophage activation. Int. J. Nanomedicine 10, 6509–6521.
Skalska, J., Frontczak-Baniewicz, M., Struzynska, L., 2015. Synaptic degeneration in rat brain after prolonged oral exposure to silver nanoparticles. Neurotoxicology 46, 145–154.
Skalska, J., Dąbrowska-Bouta, B., Strużyńska, L., 2016. Oxidative stress in rat brain but not in liver following oral administration of a low dose of nanoparticulate silver. Food Chem. Toxicol. 97, 307–315.
Skalska, J., Dąbrowska-Bouta, B., Frontczak-Baniewicz, M., Sulkowski, G., Strużyńska, L., 2020. A low dose of Nanoparticulate silver induces mitochondrial dysfunction and autophagy in adult rat brain. Neurotox. Res. 38 (3), 650–664.
Spherical Insights Global Silver Nanoparticles Market, 2023. Available from: https://www.sphericalinsights.com/reports/silver-nanoparticles-market.
Spitzer, N., Patterson, K.K., Kipps, D.W., 2021. Akt and MAPK/ERK signaling regulate neurite extension in adult neural progenitor cells but do not directly mediate disruption of cytoskeletal structure and neurite dynamics by low-level silver nanoparticles. Toxicol. In Vitro 74, 105151.
Struzynski, W., Dabrowska-Bouta, B., Grygorowicz, T., Zieminska, E., Struzynska, L., 2014. Markers of oxidative stress in hepatopancreas of crayfish (Orconectes limosus, raf) experimentally exposed to nanosilver. Environ. Toxicol. 29 (11), 1283–1291.
Sun, T.Y., Bornhöft, N.A., Hungerbühler, K., Nowack, B., 2016. Dynamic probabilistic modeling of environmental emissions of engineered nanomaterials. Environ. Sci. Technol. 50 (9), 4701–4711.
Tang, J., Xiong, L., Wang, J., Liu, L., Li, J., Wan, Z., Xi, T., 2008. Influence of silver nanoparticles on neurons and blood-brain barrier via subcutaneous injection in rats. Appl. Surf. Sci. 255, 502–504.
Tang, J., Xiong, L., Zhou, G., Wang, S., Wang, J., Liu, L., Li, J., Yuan, F., Lu, S., Wan, Z., Chou, L., Xi, T., 2010. Silver nanoparticles crossing through and distribution in the blood-brain barrier in vitro. J. Nanosci. Nanotechnol. 10 (10), 6313–6317.
Valtorta, F., Leoni, C., 1999. Molecular mechanisms of neurite extension. Philos. Trans. R. Soc. Lond. B Biol. Sci. 354 (1381), 387–394.
van der Zande, M., Vandebriel, R.J., Van Doren, E., Kramer, E., Herrera Rivera, Z., Serrano-Rojero, C.S., Gremmer, E.R., Mast, J., Peters, R.J., Hollman, P.C., Hendriksen, P.J., Marvin, H.J., Peijnenburg, A.A., Bouwmeester, H., 2012. Distribution, elimination, and toxicity of silver nanoparticles and silver ions in rats after 28-day oral exposure. ACS Nano 6 (8), 7427–7442.
van Praag, H., Christie, B.R., Sejnowski, T.J., Gage, F.H., 1999. Running enhances neurogenesis, learning, and long-term potentiation in mice. Proc. Natl. Acad. Sci. U. S. A. 96 (23), 13427–13431.
Wilson, C., Gonzalez-Billault, C., 2015. Regulation of cytoskeletal dynamics by redox signaling and oxidative stress: implications for neuronal development and trafficking. Front. Cell. Neurosci. 9, 381.
Wu, Y., Zhou, Q., 2012. Dose- and time-related changes in aerobic metabolism, chorionic disruption, and oxidative stress in embryonic medaka (Oryzias latipes): underlying mechanisms for silver nanoparticle developmental toxicity. Aquat. Toxicol. 124-125, 238–246.
Xu, F., Piett, C., Farkas, S., Qazzaz, M., Syed, N.I., 2013. Silver nanoparticles (AgNPs) cause degeneration of cytoskeleton and disrupt synaptic machinery of cultured cortical neurons. Mol. Brain 6, 29.
Yin, N., Liu, Q., Liu, J., He, B., Cui, L., Li, Z., Yun, Z., Qu, G., Liu, S., Zhou, Q., Jiang, G., 2013. Silver nanoparticle exposure attenuates the viability of rat cerebellum granule cells through apoptosis coupled to oxidative stress. Small 9 (9–10), 1831–1841.
Yu, X., Malenka, R.C., 2003. Beta-catenin is critical for dendritic morphogenesis. Nat. Neurosci. 6 (11), 1169–1177.